Journal of Catalysis **205,** 388–397 (2002)
doi:10.1006/jcat.2001.3451, available online at http://www.idealibrary.com on IDEAL®

A Periodic DFT Study of the Isomerization of Thiophenic Derivatives Catalyzed by Acidic Mordenite

Xavier Rozanska,*[,1] Rutger A. van Santen,* François Hutschka,† and Juergen Hafner‡

*Schuit Institute of Catalysis, Laboratory of Inorganic Chemistry and Catalysis, Eindhoven University of Technology, P.O. Box 513, 5600 MB Eindhoven, The Netherlands; †Département Procédés et Raffinages, TotalFina EIF, Centre Européen de Recherche et Technique, B.P. 27, 76700 Harfleur, France; and ‡Institut für Materialphysik, Universität Wien, Sensengasse 8, A-1090 Wien, Austria

Received August 23, 2001; revised October 18, 2001; accepted October 18, 2001; published online January 3, 2002

A periodic density functional theory study of the isomerization reactions of alkylated benzothiophene derivatives (i.e., dimethylated and monomethylated dibenzothiophenes and monomethylated benzotiophenes) catalyzed by acidic mordenite zeolite is reported. Monomolecular isomerization reactions have been considered and analyzed. The different reaction pathways are discussed in detail. The use of periodic structure calculations takes into consideration the electrostatic contributions and steric constraints that occur within the zeolite micropore. The isomerization reactions have been regarded as being helpful in hydrodesulfurization reactions of alkylated benzothiophene derivatives catalyzed by solid acid–metallic sulfide bifunctional catalysts. © 2002 Elsevier Science

Key Words: **acidic zeolite; mordenite; DFT calculations; quantum chemistry; transition state; desulfurization; isomerization.**

1. INTRODUCTION

Hydrodesulfurization (HDS), which decreases the sulfur content in feedstocks, is an important process in petrochemical refinery (1). New regulations have resulted in severely reducing the admitted sulfur concentration tolerance to provide more environmentally friendly fuels (1, 2).

Compounds such as thiols, thiophene, and dibenzothiophene (DBT) are not difficult to desulfurize using classical HDS catalysts (3). The catalysts used in this process are based on Mo or W sulfides, with Ni or Co promoters (1–4). However, the process is very different in alkylated benzothiophene derivatives (see Scheme 1) (3). Dibenzothiophenes, alkylated in the 4 and/or 6 positions, have been shown to be highly resistant to classical hydrodesulfurization (1–5). In the 4,6-dimethyldibenzothiophene molecule (46DMDBT), the methyl groups are supposed to prevent the thiophenic sulfur atom from being in contact with the catalytically active sites of the HDS catalyst: the two methyl groups, carbon atoms and sulfur atoms, are on the same plane (3).

[1] To whom correspondence should be addressed. Fax: 31 40 245 5054. E-mail: tgakxr@chem.tue.nl.

Hydrogenation reactions of alkylated DBT derivatives are helpful in desulfurization reactions (see Scheme 2) (3). One benzene ring of DBT becomes hydrogenated. In hydrogenated 46DMDBT, the two methyl groups, carbon atoms and thiophenic ring sulfur atoms, are no longer coplanar; hence, the sulfur atoms are in a less hindered conformation. Thus, the HDS of DBT and that of methylated DBTs have similar activities (3c).

Alternatively, the use of classical HDS and solid-acid bifunctional catalysts is proposed. The solid-acid catalyst is generally an acidic zeolite catalyst. Michaud *et al.* (5) and Landau (3a) reported that the 46DMDBT HDS reaction, which was catalyzed by a bifunctional catalyst, gave as products desulfurized isomers of this species (see Scheme 2). It is particularly interesting to form isomers from 46DMDBT, as these reactants benefit from a nonhindered sulfur atom and the inductive effect of the methyl groups, which are both facilitated by the C–S cleavage reaction (1f).

Acidic and metal-exchanged zeolite catalysts also constitute HDS catalysts. Experimental (6) and theoretical (7) studies were performed on these systems.

In this theoretical study, the isomerization reactions of methylated benzothiophene derivatives catalyzed by an acidic mordenite zeolite (H-MOR) are investigated. The mordenite (MOR) zeolite micropore structure is characterized by parallel, large 12-membered ring channels, within which large molecules such as alkylated DBTs can fit, and by smaller 8-membered ring side pockets (see Fig. 1) (8). Furthermore, acidic MOR is commercially used in petrochemistry to catalyze aromatic isomerization reactions (9). Because the molecules involved in this study are relatively large, one expects the interactions between the reactants and the zeolitic framework to play a critical role in the reactivity. Therefore, a periodic density functional theory (DFT) code was used to investigate different reaction pathways. Recent progress in methodology and highly powerful computers make full optimization as well as transition-state searches with large periodic models possible (10). The reactants that are considered in this study are alkylated DBTs that demonstrate resistance to the HDS reaction (1–5),

0021-9517/02 $35.00

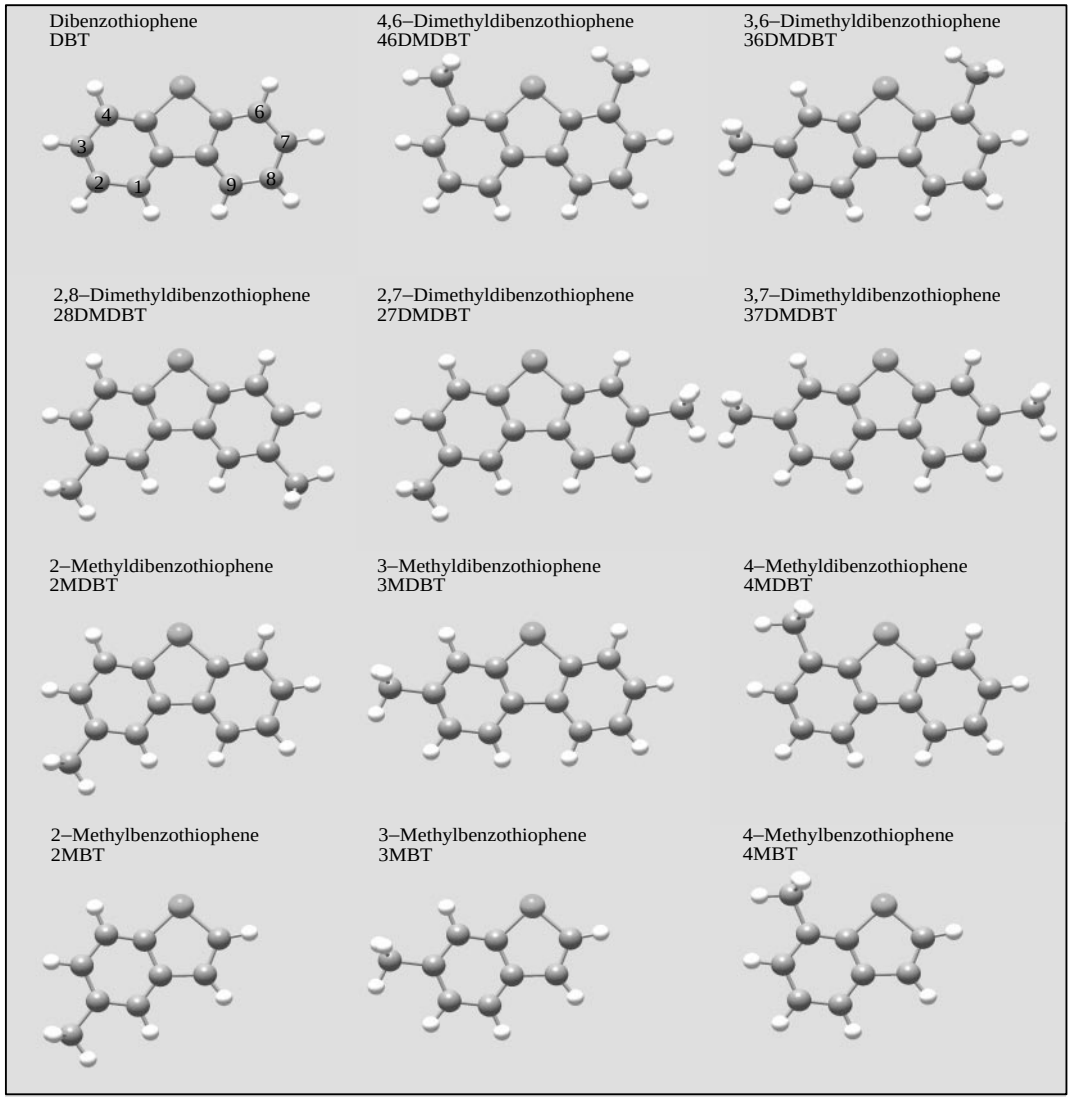

SCHEME 1. Benzothiophene derivatives.

and the reaction energy diagrams of DMDBT, MDBT, and MBT isomerization are analyzed.

2. METHOD

Periodic DFT calculations are performed using the Vienna Ab Initio Simulation Package (VASP) (11). The total energy is calculated solving the Kohn–Sham equations using the local exchange–correlation functional proposed by Perdew and Zunger (12). The results are corrected for nonlocality in the generalized gradient approximation (GGA) with the Perdew Wang 91 functional (13). VASP, which uses plane waves, and ultrasoft pseudopotentials (provided by Kresse and Hafner (14)), which are particularly well suited to significantly reducing the number of plane waves, are used. A 300-eV energy cutoff and a Brillouin-zone sampling restricted to the Γ-point are also used in our calculations.

The mordenite zeolite structure is used to perform the periodic calculations (see Fig. 1) (15). To avoid artificial interactions between the periodic images of the molecules, the minimal unit cell was doubled in the main channel direction. As a result our simulation box contains 146 atoms, with dimensions of $a = 13.648$ Å, $b = 13.672$ Å, $c = 15.105$ Å, $\alpha = 96.792^\circ$, $\beta = 90.003^\circ$, and $\gamma = 90.022^\circ$. The zeolite unit cell contains two Brønsted acid sites, and was used in previous theoretical studies (10). The acid site positions were selected at the junction of 12- and 8-membered rings. Demuth *et al.* (16a) and Brändel and Sauer (16b), reported in their theoretical studies of this zeolite, that aluminum atoms in these positions were the most stable. Relaxation of the adsorbed compounds and intermediates was performed

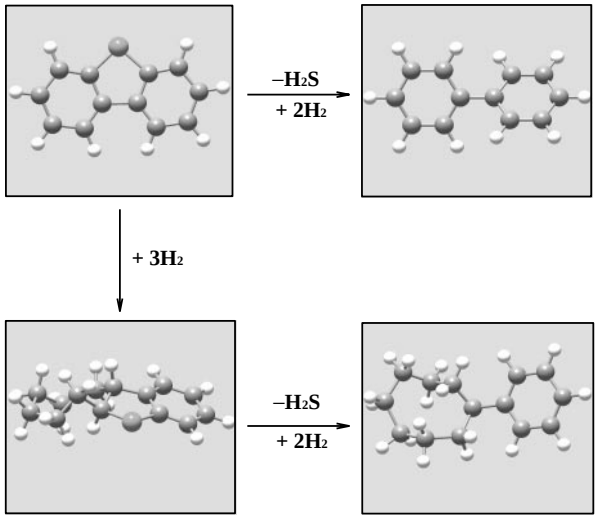

SCHEME 2. Main reaction routes for the desulfurization reaction of alkytated dibenzothiophene catalyzed by HDS catalysts (1–5).

employing a quasi-Newton algorithm based on the minimization of analytical forces. Convergence was assumed to be achieved when forces on the unit cell atoms were less than 0.05 eV/Å.

The transition-state (TS) search performed using VASP is the nudged elastic band (NEB) method (17). Several images of the system are defined along the investigated reaction pathway. These images are optimized, but only allowed to move in the direction perpendicular to the current hyper-tangent defined by the normal vector between the neighboring images. We employed up to eight images to analyze transition states. When forces on the system image atoms were below 0.08 eV/Å, the image with the maximum energy was minimized separately. In this way, artificial forces that were introduced by the elastic band were removed from the atoms.

Because the different molecules considered in this study present equivalent reactivity, the NEB method was employed only in dimethyldibenzothiophene reaction pathways analysis. The consecutively obtained TS geometries were used to estimate the transition states of methyldibenzothiophenes and methylbenzothiophenes.

3. RESULTS AND DISCUSSION

3.1. DMDBT Isomerization Reactions

The adsorption configuration mode of 46DMDBT was chosen based on experimental information. In their spectroscopic studies of the adsorption of thiophene derivatives within acidic zeolites, Garcia and Lercher (6a) and Geobaldo *et al.* (18) reported that the acidic proton was in close interaction with the thiophenic sulfur atom. Therefore, the 46DMDBT η^1(S) adsorption configuration mode with respect to the acid proton was selected (see Ads_46DMDBT in Fig. 2). The sulfur atom–acid proton distance was 2.17 Å in this system (see Table 1), and the 46DMDBT molecule protonated in the C_4 position was optimized (see C_46DMDBT in Fig. 2 and Table 2). As the forces were minimized, it was possible to check for the geometry and energy of close-to-zero-force systems (i.e., local and global minima, inflection points, and any-order saddle points). Protonated aromatics within acidic zeolites have been demonstrated to correspond to an

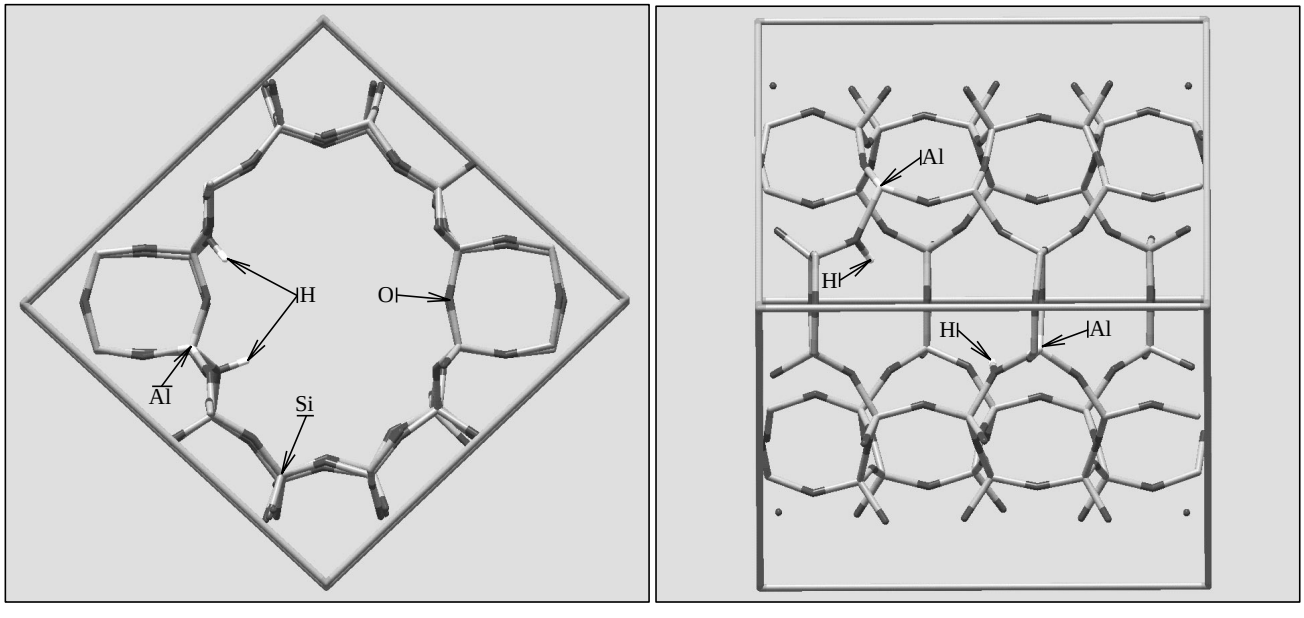

FIG. 1. The mordenite unit cell which was used in this study. Mordenite zeolite is characterized by parallel, large 12-membered ring channels that have 8-membered ring side pockets along their axes.

TABLE 1

Geometries of the Alkylated Benzothiophene Derivatives Adsorbed within Acidic Mordenite as Obtained from the Periodical Structure Calculations[a]

	Ads_46DMDBT	Ads_36DMDBT	Ads_37DMDBT	Ads_4MDBT	Ads_3MDBT	Ads_4MBT	Ads_3MBT
AlO_1	1.91	1.91	1.91	1.91	1.91	1.91	1.91
AlO_2	1.69	1.69	1.69	1.69	1.69	1.69	1.69
AlO_3	1.69	1.69	1.69	1.69	1.69	1.69	1.69
AlO_4	1.7	1.7	1.71	1.7	1.7	1.7	1.7
O_1H_a	1.02	1.02	1.02	1.01	1.01	1.01	1.01
H_aS	2.17	2.18	2.18	2.18	2.18	2.2	2.2
AlO_1H_a	112.8	112.7	112.7	112.7	112.6	112.5	112.5
O_1H_aS	165	165	164.8	164.9	164.6	164.9	164.7
$O_1H_aC_1$	154.8	154.8	154.3	154.8	154.7	154.9	154.9
$O_1H_aC_2$	154.4	154.4	154.7	154.6	154.6	155	154.9

[a] Distances are in Å, and angles are in degrees.

unstable situation (19). Moreover, such protonation steps were recently analyzed by periodic structure DFT calculations and did not correspond to first-order transition states (20). Similar results were obtained in the case of 46DMDBT. The energy constantly increased from Ads_46DMDBT to C_46DMDBT, during the protonation reaction of the molecule, with the energy of C_46DMDBT being +57 kJ/mol with respect to Ads_46DMDBT.

In previous studies (20, 21), we investigated all possible pathways for aromatic isomerization. Some of these reaction pathways require the aromatic molecule to reorientate itself with respect to the catalytic active site so that it could be followed. Due to its large size, the DMDBT molecule has a limited ability to reorientate itself within the mordenite micropore. As a result, isomerization can occur only through an intramolecular shift isomerization reaction without further reorientation of the molecules. The occurrence of intermolecular reactions of alkylated benzothiophene derivatives is impossible within mordenite zeolite, as the corresponding transition states and intermediates

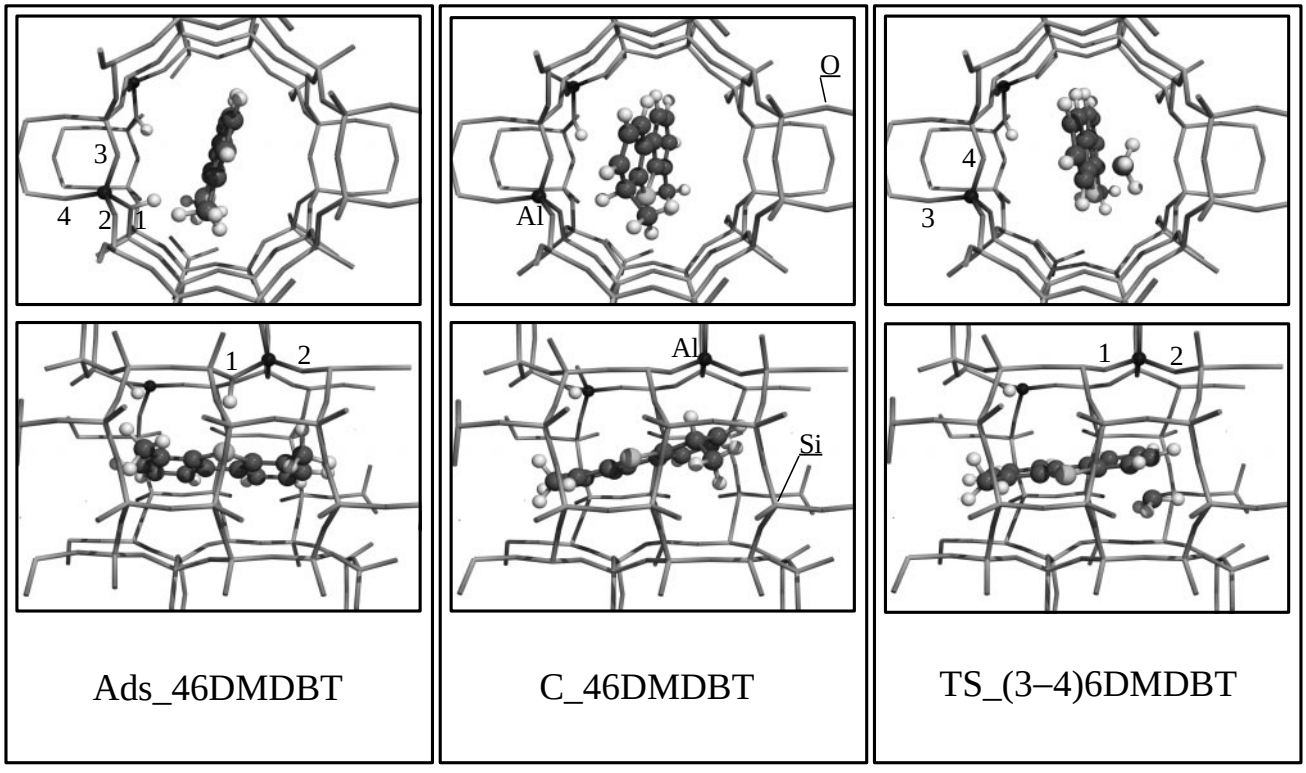

FIG. 2. 46DMDBT geometries adsorbed to the acidic site (Ads_46DMDBT), transient protonated 46DMDBT (C_46DMDBT), and the shift isomerization TS of 46DMDBT into 36DMDBT (TS_(3–4)6DMDBT) as obtained from the periodic calculations.

TABLE 2

Protonated 46DMDBT Geometries within Acidic Mordenite as Obtained from the Periodical Structure Calculations[a]

	C_46DMDBT
AlO_1	1.75
AlO_2	1.73
AlO_3	1.72
AlO_4	1.71
O_1H_a	2.11
O_2H_a	2.71
H_aC_4	1.12
C_4C_{m1}	1.55
$O_1H_aC_4$	164.2
$O_2H_aC_4$	121.5
$C_3C_5C_4C_{m1}$	129.1
$C_3C_5C_4H_a$	−117.4

[a] Distances are in Å, and angles are in degrees.

TABLE 3

Isomerization Transition State Geometries of the Alkylated Benzothiophene Derivatives Catalyzed by Acidic Mordenite as Obtained from the Periodical Structure Calculations[a,b]

	TS_(3–4)6 DMDBT	TS_3(6–7) DMDBT	TS_(3–4) MDBT	TS_(3–4) MBT
AlO_1	1.73	1.73	1.73	1.73
AlO_2	1.73	1.73	1.73	1.73
AlO_3	1.72	1.72	1.72	1.72
AlO_4	1.73	1.73	1.73	1.73
$C_{m1}C_a$	1.92	1.92	1.93	1.91
$C_{m1}C_b$	1.92	1.92	1.91	1.92
$C_{m1}C_aC_b$	67.9	67.9	67.4	68.5
$C_{m1}C_bC_a$	68.2	68.3	68.8	67.7
C_aO_1	4.38	4.38	4.38	4.39
C_aO_2	4.51	4.49	4.50	4.51
C_aO_3	4.17	4.17	4.17	4.18
C_bO_1	4.87	4.87	4.87	4.86
C_bO_2	4.40	4.39	4.40	4.40
C_bO_3	3.76	3.76	3.76	3.76

[a] Distances are in Å, and angles are in degrees.

[b] C_{m1} is the label for the carbon atom of the shifting methyl group. C_a and C_b are the carbon atoms that belong to the aromatic ring to which the shifting methyl was connected (C_a) and to which it will be connected (C_b). For TS_(3–4)6DMDBT, C_a is C_4 and C_b is C_3, respectively.

involved in these reactions are too large to fit into the parallel channels (22). We have previously shown that alkylated aromatics (i.e., xylene molecules) preferably convert through a shift isomerization reaction consecutive to the protonation step, and highly nonalkylated aromatics (i.e., toluene) can convert *via* different shift isomerization reaction pathways within mordenite (20). In benzothiophene derivatives, isomerization *via* a dealkylation reaction of alkylated aromatics with the formation of a methoxy intermediate cannot occur easily (20). To follow this reaction pathway, the protonated 46DMDBT molecule must make a 180° rotation within the ellipsoidal 12-membered ring channel of mordenite zeolite.

The transition-state geometry of the shift isomerization from 46DMDBT to 36DMDBT is shown in Fig. 2 (see TS_(3–4)6DMDBT). In this transition state, the shifting methyl group is located in an intermediate location between the C_4 and the C_3 atom ($C_{m1}C_4 = 1.92$ Å, $C_{m1}C_3 = 1.92$ Å, $C_{m1}C_4C_3 = 67.9°$ and $C_{m1}C_3C_4 = 68.2°$) (see Table 3). The TS takes place relatively far from the deprotonated Brønsted acid site (see Table 3), but is actually stabilized by the oxygen atoms, which are situated on the opposite side of the 12-membered ring channel with respect to the Brønsted acid site, that belong to the 8-membered ring side pocket opening (see Figs. 2 and 3). As can be seen in Fig. 3, the shifting methyl group hydrogen atoms and the 8-membered

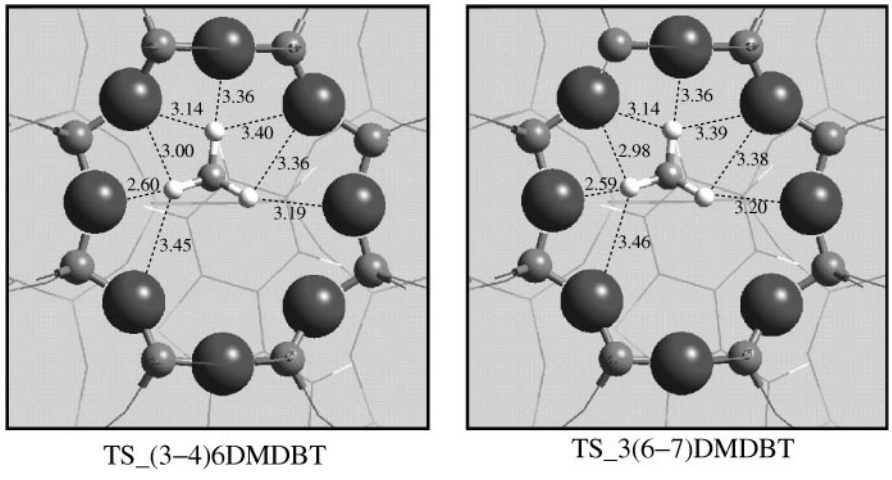

FIG. 3. Details of the shift isomerization TS geometries. The shifting methyl group is in close interaction with the oxygen atoms of the eight-membered ring.

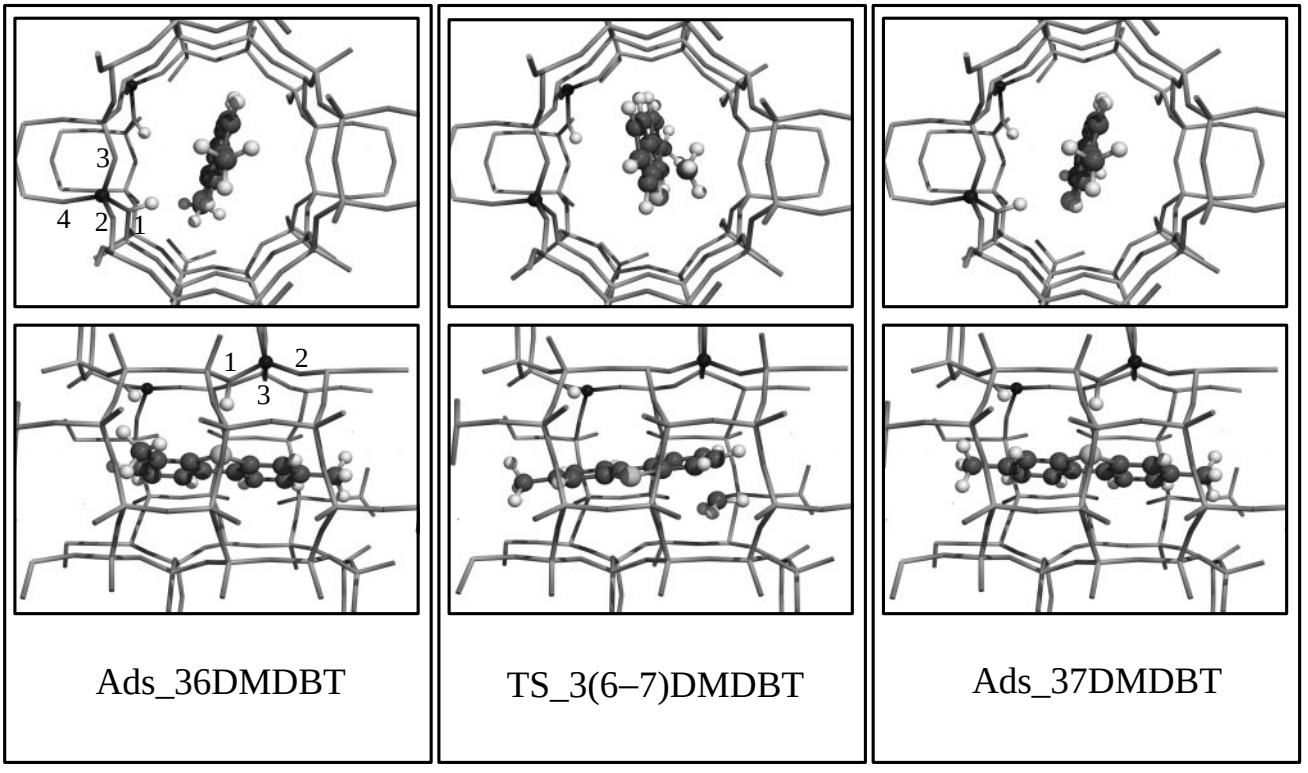

FIG. 4. 36DMDBT geometries adsorbed to the acidic site (Ads_36DMDBT), the shift isomerization TS of 36DMDBT into 37DMDBT (TS_3(6-7)DMDBT), and 37DMDBT adsorbed to the acidic site (Ads_37DMDBT) as obtained from the periodic calculations.

ring oxygen atoms are involved in the formation of several weak hydrogen bonds. The computed activation energy of this reaction with respect to Ads_46DMDBT is $E_{act} = +137$ kJ/mol. Following the shift isomerization, the proton on the DMDBT molecule is back-donated without an activation energy barrier to the deprotonated Brønsted acid site (19, 20).

Following the previous isomerization reaction, 36DMDBT is formed (see Ads_36DMDBT in Fig. 4). In the DMDBT isomer, only the η^1(S) adsorption mode was investigated. The location of the 36DMDBT molecule with respect to the acidic site is very similar to that of the 46DMDBT molecule (see Table 1). However, the energy level of this system is 18 kJ/mol below that of Ads_46DMDBT. This energy difference comes from the less sterically hindered alkylated DBT isomer within the mordenite channel. The shifted methyl group now points to the same direction as the 12-membered ring channel and is no longer in close contact with the zeolite framework atoms.

In 36DMDBT, the reverse isomerization reaction that leads to the formation of 46DMDBT is more difficult than the opposite reaction: the activation energy is $E_{act} = +155$ kJ/mol with respect to Ads_36DMDBT. On the other hand, the isomerization reaction into 37DMDBT that proceeds *via* a mechanism similar to that in TS_(3– 4) 6DMDBT has a lower activation energy, i.e., +142 kJ/mol with respect to Ads_36DMDBT (see TS_3(6–7)DMDBT in Figs. 3 and 4). Such an activation energy difference ($\Delta E_{act} = 13$ kJ/mol) is considered to be sufficient enough to induce the preference of one reaction against another (23). Therefore, after 46DMDBT is isomerized into 36DMDBT, it is unlikely that further reactions would regenerate it.

The position of the methyl group that does not participate in the isomerization reaction seems to have very limited influence on TS_3(6–7)DMDBT in comparison to TS_(3–4)6DMDBT. The two TS geometries are very similar (see Table 3) regarding the activation energies with respect to their corresponding ground states ($E_{act} = +137$ for TS_(3–4)6DMDBT and +142 kJ/mol for TS_3(6–7) DMDBT).

The isomerization reaction of the 36DMDBT molecule according to the mechanism depicted in TS_3(6–7)DMDBT leads to the formation of 37DMDBT (see Ads_37DMDBT in Fig. 4, and Table 1). This DMDBT isomer shows a similar position to that of 46DMDBT and 36DMDBT with respect to the Brønsted acid site. However, adsorbed 37DMDBT is 14 and 32 kJ/mol more stable than adsorbed 36DMDBT and adsorbed 46DMDBT, respectively. The isomerization reaction of 37DMDBT into 36DMDBT has a similar activation energy to that of 36DMDBT into 46DMDBT ($E_{act} = +156$ and +155 kJ/mol, respectively).

We did not consider further isomerization reactions of 37DMDBT for two reasons. First, the isomerization

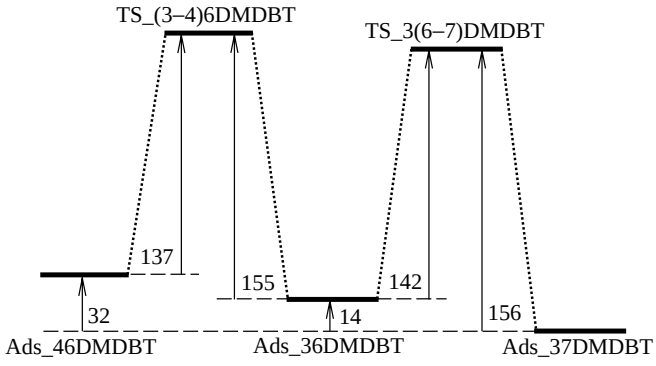

FIG. 5. Reaction energy diagram of dimethyldibenzothiophene isomerization (DMDBT) catalyzed by acidic mordenite. The values correspond to 0 K energy in kilojoule per mole.

reactions of 37DMDBT into 27DMDBT and 28DMDBT have not been shown to occur (5). Second, the sizes of the 27DMDBT and 28DMDBT molecules are similar to those of 36DMDBT and 46DMDBT (see Scheme 1). Therefore, one can assume that the energy level of the adsorbed 28DMDBT and 27DMDBT and the reactivity of these molecules are similar to those of 46DMDBT and 36DMDBT. In order to support this assumption, the energy of the adsorbed state of 27DMDBT within the mordenite system has been calculated. It is found to be +19 kJ/mol with respect to Ads_37DMDBT.

The reaction energy diagram of the isomerization reaction of the DMDBT molecules is shown in Fig. 5. As can be seen in this figure, the isomerization reaction of 46DMDBT into more easily desulfurized isomers is a favorable reaction. Moreover, the differences in the diffusivity of alkylated DBTs can also play an important role in the source of the selectivity (8). In DMDBT isomerization catalyzed by acidic mordenite, another effect favors 37DMDBT selectivity. The adsorption behavior of the different DMDBT isomers on the catalytic active site has a clear discriminating effect. Indirectly, this difference in adsorption behavior induces transition-state selectivity (9a, 24): in 36DMDBT, the isomerization reaction toward 37DMDBT is preferred over that toward 46DMDBT, despite the fact that TS_(3–4)6DMDBT and TS_3(6–7)DMBT show the same intrinsic difficulty for conversion.

3.2. MDBT and MBT Isomerization Reactions

In this section, the monomethylated DBT and MBT isomerization reactions are described. These compounds, when alkylated in the C_4 position, have experimentally been more desulfurization resistant than other alkylated isomers (3c). Moreover, because the sizes of these molecules are different from those of the DMDBT isomers, they can be used to check the reactivity of different reactants within a given acidic zeolite catalyst for a given reaction mechanism. It was clearly shown that reactivity and selectivity within zeolite catalysts are strongly dependent on the dimension and structure of the micropore channels as well as those of the reactants and reactions considered (24).

As described previously, the η^1(S) adsorption mode of 4MDBT was selected among all others as the initial estimated geometry (see Ads_4MDBT in Fig. 6 and Table 1). Interestingly, the H_aS distance for MDBT is similar to that for the DMDBT molecules (H_aS = 2.18 Å) (see Table 1). The methyl groups do not affect the position of the benzothiophene derivatives much with respect to the Brønsted acid site. This indicates that the thiophenic sulfur atom position with respect to the acid proton is of more importance in the location of the energy minima than the positions of the methyl groups. The different alkylated positions in the DMDBT or MDBT molecules do not even change the position of the sulfur atom as a function of the acid proton; however, they have an important energetic effect. Moreover, one notes that the S···O interactions are less favorable than the H···O interactions.

In 4MDBT, isomerization can occur after protonation. The TS geometry that leads from 4MDBT to the formation of 3MDBT is shown in Fig. 6 (see TS_(3–4)MDBT). The activation energy barrier of this reaction is E_{act} = +151 kJ/mol with respect to Ads_4MDBT. As for DMDBTs in this transition state, the shifting methyl is stabilized by the oxygen atoms of the eight-membered ring structure (see Fig. 7).

A comparison of the MDBT isomerization reaction to a similar reaction of the DMDBT molecules (i.e., Ads_46DMDBT → TS_(3–4)6DMDBT and Ads_36DMDBT → TS_3(6–7)DMDBT) shows that the activation energy barrier is around 10 kJ/mol higher.

TS_(3–4)MDBT gives as product a 3MDBT molecule. The adsorption of this molecule within the acidic mordenite channel is 13 kJ/mol more stable than that of the 4MDBT molecule. The reverse isomerization reaction of 3MDBT into 4MDBT presents an activation energy barrier of E_{act} = +164 kJ/mol. The reaction energy diagram of the MDBT isomerization reaction is displayed in Fig. 8.

Compared to DMDBT, MDBT isomerization reactions are more difficult (ΔE_{act} is around 10 kJ/mol), whereas the ordering of the isomerized adsorbed dibenzothiophene derivatives remains very similar.

In the following the methylbenzothiophene isomerization reactions are considered. After 4MBT adsorbs to the Brønsted acid site (see Ads_4MBT in Fig. 9), the isomerization reaction proceeds as with the previous alkylated benzothiophene derivatives. For 4MBT, the distance for the acid proton–thiophenic sulfur atom is longer than that for the DMDBT or MDBT molecules (H_aS = 2.2 Å *versus* 2.18 Å) (see Table 1). Interestingly, it is with the smaller benzothiophene molecule that one obtains the longest H_aS distance. This supports the importance of the sulfur–acid proton hydrogen bond *versus* the hydrogen bonds between

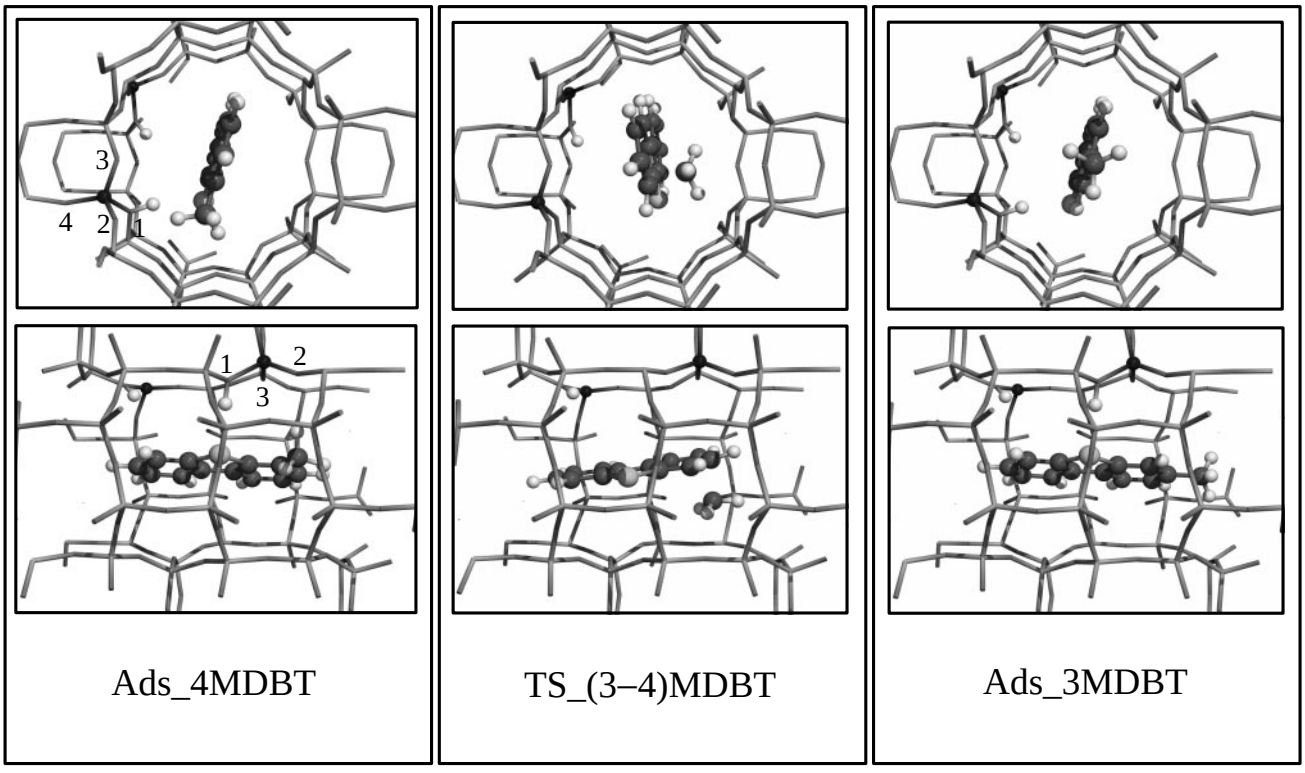

FIG. 6. 4MDBT geometries adsorbed to the acidic site (Ads_4MDBT), the shift isomerization TS of 4MDBT into 3MDBT (TS_(3–4)MDBT), and 3MDBT adsorbed to the acidic site (Ads_3MDBT) as obtained from the periodic calculations.

the methyl group hydrogen atoms and the zeolite oxygen atoms.

The TS geometry that occurs from Ads_4MBT is shown in Figs. 9 and 10 (see TS_(3–4)MBT). The shifting methyl group is located slightly closer to the C_4 atom than in the case of the DMDBT shift isomerization reactions (in TS_(3–4)MBT geometry, $C_{m1}C_4 = 1.91$ Å, $C_{m1}C_3 = 1.92$ Å, $C_{m1}C_4C_3 = 68.5°$, and $C_{m1}C_3C_4 = 67.7°$) (see Table 3). The activation energy barrier of the 4MBT to 3MBT isomerization reaction is $E_{act} = +134$ kJ/mol with respect to Ads_4MBT. Compared to the similar reactions obtained for DMDBT and MDBT derivatives, this activation energy barrier is around 5 and 15 kJ/mol lower, respectively.

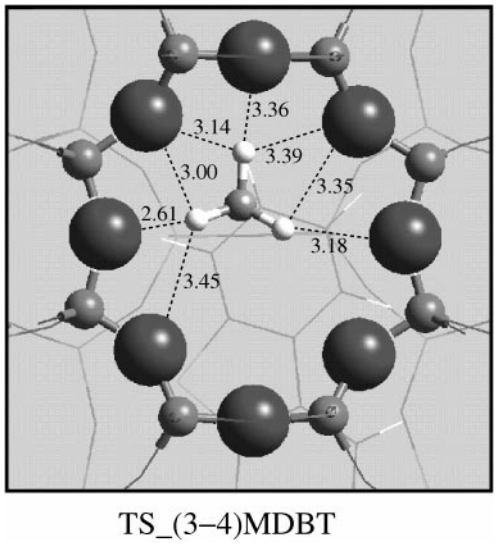

FIG. 7. Details of the shift isomerization TS geometry (TS_(3–4)MDBT).

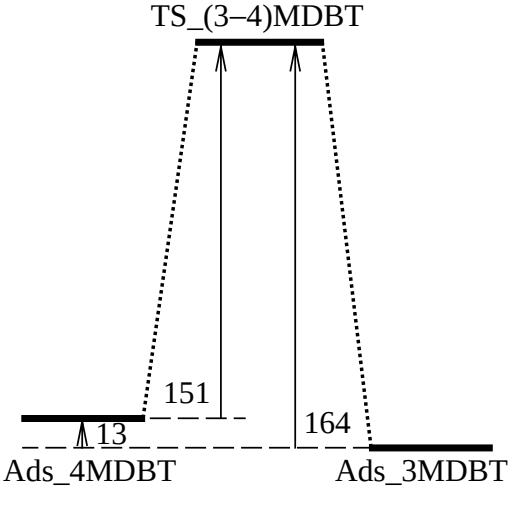

FIG. 8. Reaction energy diagram of the methyldibenzothiophene isomerization (MDBT) catalyzed by acidic mordenite. The values correspond to 0 K energy in kilojoule per mole.

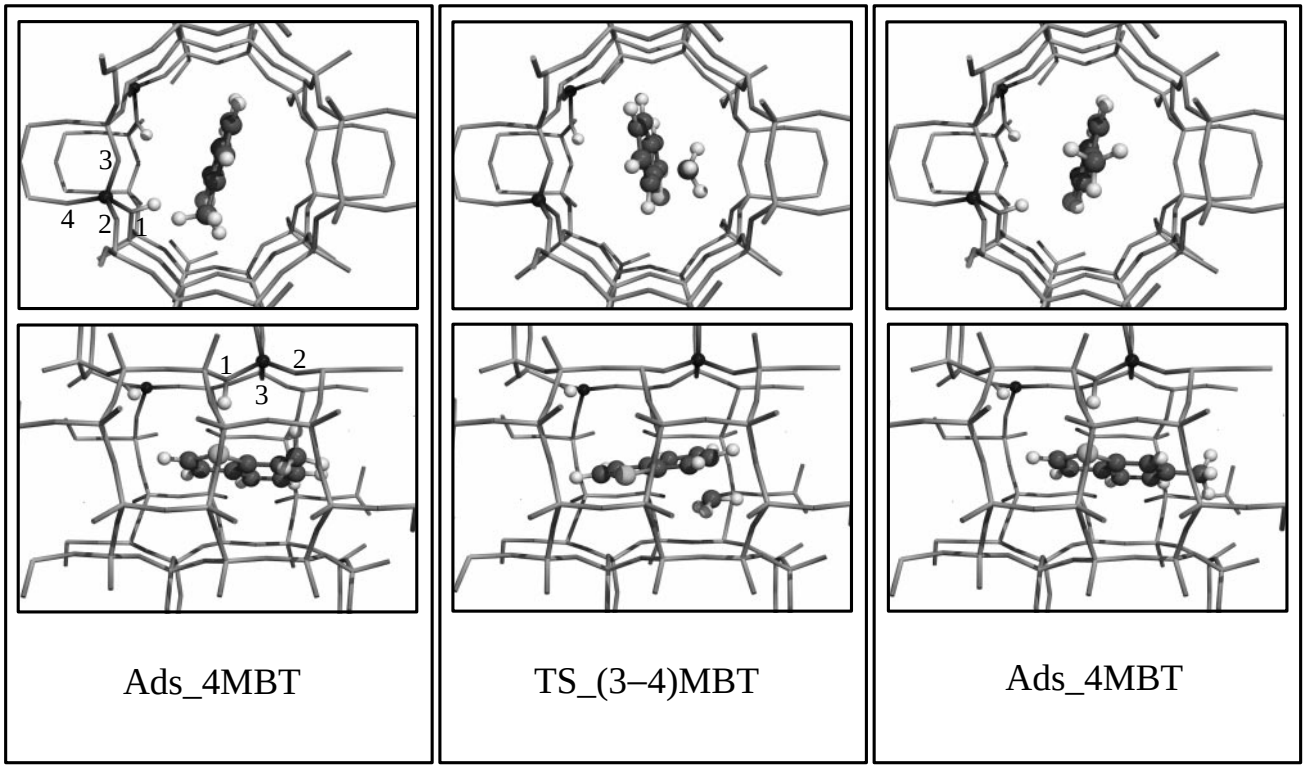

FIG. 9. 4MBT geometries adsorbed to the acidic site (Ads_4MBT), the shift isomerization TS of 4MBT into 3MBT (TS_(3–4)MBT), and 3MBT adsorbed to the acidic site (Ads_3MBT) as obtained from the periodic calculations.

The energy level of 3MBT adsorbed within the acidic mordenite channel is 12 kJ/mol below that of Ads_4MBT. The geometry of adsorbed 3MBT is described in Table 1 and Fig. 9 (see Ads_3MBT). The reaction energy diagram of the shift isomerization reaction of MBT is plotted in Fig. 11.

In summary, it appears that the isomerization activation energies do not correlate with the size of the benzothiophene derivatives. On the contrary, the differences in activation energies obtained in the DMDBT, MDBT, and MBT molecules can only be explained by taking into consideration the intrinsic chemical properties of the different derivatives. In MDBT, MBT, and DMDBT molecules, the

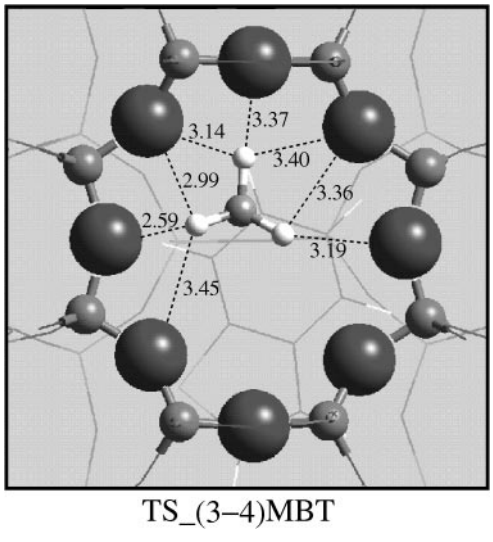

FIG. 10. Details of the shift isomerization TS geometry (TS_(3–4)MBT).

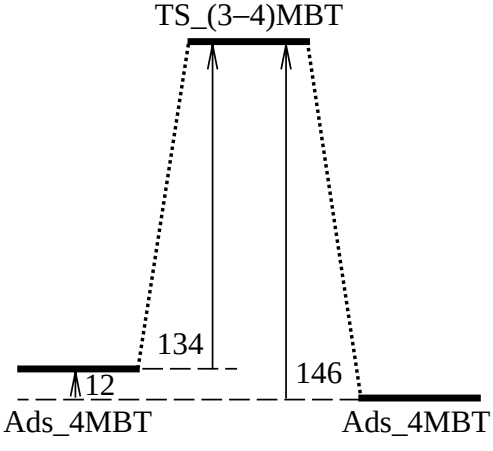

FIG. 11. Reaction energy diagram of methylbenzothiophene isomerization (MBT) catalyzed by acidic mordenite. The values correspond to 0 K energy in kilojoule per mole.

adsorption behavior of the reactants to the catalytic active site can explain the origin of the reaction selectivity. However, it must be remembered that the structure of mordenite zeolite determines this result, as the parallel channels favor the adsorption of benzothiophene derivatives alkylated in the C_3 and/or C_4 position(s). Other zeolite micropore structures will lead to different adsorption behavior and therefore different reaction selectivity (24).

4. CONCLUSIONS

In this paper, a theoretical study of isomerization reactions of alkylated benzothiophene derivatives catalyzed by acidic mordenite has been presented. Reaction energy diagrams of the reaction and estimates of the activation energy barriers are provided. The results indicate that isomerization reactions of alkylated benzothiophene derivatives in the 4 and/or 6 positions will lead to selective reactions to other isomers in which the thiophenic sulfur atom is not hindered by the methyl group(s). This confirms the experimental results of an enhanced activity of HDS bifunctional catalysts in the desulfurization reactions of 46DMDBT or 4MDBT (3a, 5).

The calculations were made by using a periodic structure DFT program which allows consideration of the zeolite framework. Interestingly, it appears in the case of the system described in this study that transition state selectivity for isomerization reactions is induced by the adsorption behavior of the molecules, and the transition states are energetically similar with respect to the adsorption configuration that leads to reaction.

ACKNOWLEDGMENTS

Computational resources have been partly granted by the Dutch National Computer Facilities (NCF). This work was performed within the European Research Group Ab Initio Molecular Dynamics Applied to Catalysis and supported by the Centre National de la Recherche Scientifique (CNRS), the Institut Français du Pétrole (IFP), and the TotalFina Raffinage Distributions company. XR is grateful to TotalFina Raffinage Distributions for financial support.

REFERENCES

1. (a) Sullivan, D. L., and Ekerdt, J. G., *J. Catal*. **178**, 226 (1998); (b) Miciukiewicz, J., Laniecki, M., and Domka, F., *Catal. Lett*. **51**, 65 (1998); (c) Zhang, Y., Wei, Z., Yan, W., Ying, P., Ji, C., Li, X., Zhou, Z., Sun, X., and Xin, Q., *Catal. Today* **30**, 135 (1996); (d) Logan, J. W., Heiser, J. L., McCrea, K. R., Gates, B. D., and Bussel, M. E., *Catal. Lett*. **56**, 165 (1998); (e) Kabe, T., Qian, W., Wang, W., and Ishihara, A., *Catal. Today* **29**, 197 (1996); (f) Segawa, K., Takahashi, K., and Satoh, S., *Catal. Today* **63**, 123 (2000).
2. (a) Knudsen, K. G., Cooper, B. H., and Topsøe, H., *Appl. Catal. A* **189**, 205 (1999); (b) Takatsuka, T., Inoue, S.-I., and Wada, Y., *Catal. Today* **39**, 69 (1997).
3. (a) Landau, M. V., *Catal. Today* **36**, 393 (1997); (b) Landau, M. V., Berger, D., and Herskowitz, M., *J. Catal.* **158**, 236 (1996); (c) Meille, V., Schulz, E., Lemaire, M., and Vrinat, M., *J. Catal.* **170**, 29 (1997).
4. Bianchini, C., and Meli, A., *in* "Transition Metal Sulphides, Chemistry and Catalysis" (T. Weber, R. Prins, and R. A. van Santen, Eds.), NATO ASI Serie 3, Vol. 60, p. 129. Kluwer Academic, Dordrecht, 1998.
5. Michaud, P., Lemberton, J. L., and Pérot, G., *Appl. Catal. A* **169**, 343 (1998).
6. (a) Garcia, C. L., and Lercher, J. A., *J. Mol. Struct.* **293**, 235 (1993); (b) Welters, W. J. J., De Beer, V. H. J., and Van Santen, R. A., *Appl. Catal. A* **119**, 253 (1994); (c) Welters, W. J. J., Vorbeck, G., Zandberger, H. W., De Haan, J. W., De Beer, V. H. J., and Van Santen, R. A., *J. Catal.* **150**, 155 (1994).
7. (a) Saintigny, X., Van Santen, R. A., Clémendot, S., and Hutschka, F., *J. Catal.* **183**, 107 (1999); (b) Rozanska, X., Van Santen, R. A., Hutschka, F., *J. Catal.* **200**, 79 (2001).
8. Waghmode, S. B., Bharathi, P., Sivasanker, S., and Vetrivel, R., *Microporous Mesoporous Mater*. **38**, 433 (2000).
9. (a) Venuto, P. B., *Microporous Mater.* **2**, 297 (1994); (b) Hölderich, W. F., and Van Bekkum, H., *in* "Introduction to Zeolite Science and Practice" (H. van Bekkum, E. M. Flaningen, and J. C. Jansen, Eds.), Vol. 58, p. 631. Elsevier, Amsterdam, 1991.
10. Vos, A. M., Rozanska, X., Schoonheydt, R. A., Van Santen, R. A., Hutschka, F., and Hafner, J., *J. Am. Chem. Soc*. **123**, 2799 (2001).
11. (a) Kresse, G., and Hafner, J., *Phys. Rev. B* **48**, 13,115 (1993); (b) Kresse, G., and Hafner, J., *Phys. Rev. B* **49**, 14,251 (1994); (c) Kresse, G., and Furthmüller, J., *Comput. Matter Sci.* **6**, 15 (1996); (d) Kresse, G., and Furthmüller, J., *Phys. Rev. B* **54**, 11,169 (1996).
12. Perdew, J. P., and Zunger, A., *Phys. Rev. B* **23**, 5048 (1981).
13. Perdew, J. P., Burke, K., and Wang, Y., *Phys. Rev. B* **54**, 16,533 (1996).
14. Kresse, G., and Hafner, J., *J. Phys. Condens. Matter* **6**, 8245 (1994).
15. (a) Barrer, R. M., and White, E. A. D., *J. Chem. Soc.* **2**, 1561 (1952); (b) Meier, W. M., *Z. Kristallogr*. **115**, 439 (1961); (c) Rouse, R. C., and Peacor, D. R., *Am. Mineral* **79**, 175 (1994).
16. (a) Demuth, T., Hafner, J., Benco, L., and Toulhoat, H., *J. Phys. Chem. B* **104**, 4593 (2000); (b) Brändel, M., and Sauer, J., *J. Am. Chem. Soc.* **120**, 1556 (1998).
17. Mills, G., Jónsson, H., and Schenter, G. K., *Surf. Sci.* **324**, 305 (1995).
18. Geobaldo, F., Palomino, G. T., Bordiga, S., Zecchina, A., and Areán, C. O., *Phys. Chem. Chem. Phys.* **1**, 561 (1999).
19. Paukshtis, E. A., Malysheva, L. V., and Stepanov, V. G., *React. Kinet. Catal. Lett.* **65**, 145 (1998).
20. Rozanska, X., Van Santen, R. A., Hutschka, F., and Hafner, J., *J. Am. Chem. Soc*. **123**, 7655 (2001).
21. Rozanska, X., Saintigny, X., Van Santen, R. A., and Hutschka, F., *J. Catal*. **202**, 141 (2001).
22. (a) Corma, A., and Sastre, E., *J. Catal.* **129**, 177 (1991); (b) Halgeri, A. B., and Das, J., *Appl. Catal. A* **181**, 347 (1999).
23. Corma, A., Sastre, G., and Viruella, P. M., *J. Mol. Catal. A* **100**, 75 (1995).
24. (a) Tsai, T.-C., Liu, S.-B., and Wang, I., *Appl. Catal. A* **181**, 355 (1999); (b) Fraenkel, D., and Levy, M., *J. Catal.* **118**, 10 (1989).